Efficient magnonic transport and domain wall landscape of insulating antiferromagnetic thin films

Andrew Ross[1,2,*], Romain Lebrun[1,*,†], Olena Gomonay[1], Daniel A. Grave[3], Asaf Kay[3], Lorenzo Baldrati[1], Sven Becker[1], Alireza Qaiumzadeh[4], Camilo Ulloa[5], Gerhard Jakob[1,2], Florian Kronast[6], Jairo Sinova[1,7], Rembert Duine[4,5,8], Arne Brataas[4], Avner Rothschild[3], Mathias Kläui[1,2,4,†]

1. *Institut für Physik, Johannes Gutenberg Universität-Mainz, 55099, Mainz, Germany*
2. *Graduate School of Excellence Materials Science in Mainz (MAINZ), Staudinger Weg 9, 55128, Mainz, Germany*
3. *Department of Materials Science and Engineering, Technion-Israel Institute of Technology, Haifa 32000, Israel*
4. *Center for Quantum Spintronics, Department of Physics, Norwegian University of Science and Technology, Trondheim, Norway*
5. *Institute for Theoretical Physics, Utrecht University, Princetonplein 5, 3584 CC Utrecht, The Netherlands*
6. *Helmholtz-Zentrum Berlin für Materialen und Energie, Albert-Einstein-Straße 15, D-12489 Berlin, Germany*
7. *Insitute of Physics ASCR, v.v.i., Cukrovarnicka 10, 162 53 Praha 6 Czech Republic*
8. *Department of Applied Physics, Eindhoven University of Technology, P.O. Box 513, 5600 MB Eindhoven, The Netherlands*

Abstract:

Spintronics seeks to functionalize antiferromagnetic materials to develop memory and logic devices operating at terahertz speed and robust against external magnetic field perturbations. To be useful, such functionality needs to be developed in *thin film* devices. The key functionality of long-distance spin-transport has, however, so far only been reported in *bulk* single crystal antiferromagnets, while in thin films, transport has so far been limited to a few nanometers.

In this work, we electrically achieve a long-distance propagation of spin-information in thin films of the insulating antiferromagnet hematite. Through transport and magnetic imaging, we demonstrate a strong correlation between the efficiency of the transport of magnons, which carry spin-information, and the magnetic domain structure of the films. In thin films with large domains, magnons propagate over micrometer distances whilst they attenuate over much shorter distances in multidomain thin films. The governing factor of the attenuation is related to scattering at domain walls, and we demonstrate that we can reduce this through training by field

* These authors contributed equally to this work. † Corresponding authors: rolebrun@uni-mainz.de, klaeui@uni-mainz.de

cyclings. For the appropriate crystalline orientation of the films, spin-transport is achieved in zero applied field across micrometers, as required for integration with devices.

Recently, the focus of spintronics research has been shifting towards utilizing antiferromagnetic materials, with benefits over ferromagnets including terahertz spin dynamics and high stability against applied external magnetic fields[1,2]. Beyond reading[3,4] and switching[5,6] of the antiferromagnetic order, the efficient transport of spin-information has only been demonstrated in a mm thick single crystal of the easy-axis antiferromagnet hematite[7]. However, in thin film antiferromagnets, as required for the development of spintronic devices and back-end integration with current CMOS technologies, spin-information was previously shown to propagate across only a few nanometers in both insulating[8,9] and metallic[10] antiferromagnets.

Spin-transport in antiferromagnetic insulators occurs through the excitation of the magnetic order, and the propagation of spin-waves, also known as magnons. Antiferromagnetic magnons can be either linearly- or circularly-polarized. However, only circularly-polarized magnon modes, present in antiferromagnets with an easy-axis anisotropy, carry angular momentum, permitting the transport of spin-information[11]. The spin-information of these magnons is carried (anti-)parallel to the equilibrium orientation of the antiferromagnetic Néel vector, $\boldsymbol{n}$[7] . The propagation of antiferromagnetic magnons can be monitored in an adjacent heavy metal layer acting as the source of detection and of excitation[7,12]. The generated signal strength is proportional to $\propto (\boldsymbol{n} \cdot \boldsymbol{\mu}_S)^2$, where $\boldsymbol{\mu_s}$ is the spin-accumulation in the heavy metal, leading to a maximal efficiency for $\boldsymbol{n}||\boldsymbol{\mu_s}$. The additional application of an external magnetic field, **H**, can be used to manipulate the direction of $\boldsymbol{n}$ with respect to $\boldsymbol{\mu_s}$ and also serves to tune the frequencies of the contributing magnons. In particular in an easy-axis (**EA**) antiferromagnet, $\mathbf{H}||\hat{z}$(**EA**) leads to the well-known spin-flop transition, with the presence of a soft magnon mode[12,13] and by which the magnons undergo a transition from circular to linear polarization.

A particularly promising antiferromagnetic material for spin-transport is the iron oxide hematite, α-Fe_2O_3, an ubiquitous antiferromagnet commonly used in applications as diverse as humidity sensors[14] and photoelectrochemical cells[15]. Beyond these applications, it is also a promising material for spintronic devices, given its low magnetic damping and intrinsic micrometer spin-diffusion length in

bulk single crystals[7]. Hematite is also unique for its well-known Morin phase transition (MT)[16], where it undergoes a transition at a temperature T_M from an easy-axis phase along the (0001) c-axis[17] to an easy-plane phase where the magnetic moments lie perpendicular to (0001) ($T_M \sim 260$ K in undoped bulk crystals). While long-distance spin-transport has been studied in bulk hematite[7], such bulk crystals are incompatible with use in devices. The practical solution would be to utilize thin film antiferromagnets. However, so far the evaluated spin-diffusion lengths have been found to be too short for useful applications. It is, however, unclear what mechanism is preventing the long-distance transport of magnons in thin film antiferromagnets. In particular, as the low magnetic damping should lead to long spin-diffusion lengths also in thin films, one needs to understand why these have so far not been observed and how one can realize the potential of this materials class in an applications-relevant thin film setting.

In this work, we address these open questions by realizing long-distance magnon transport in a thin film antiferromagnetic system and we identify the mechanisms governing the magnon propagation length by a systematic study. As the materials system, we emply epitaxial α-Fe_2O_3 thin films grown on sapphire substrates with different surface plane orientations[18,19]. The magnon propagation is investigated in these films as a function of applied field relative to the magnetic symmetry axes allowing for the extraction of the magnon propagation lengths of the different samples. To unravel the origin of the differences in the observed spin-transport length scales, the antiferromagnetic domain structure of the same films is determined by direct imaging and we identify, in conjunction with theoretical calculations, scattering at domain walls as the governing factor for the propagation.

First, we consider α-Fe_2O_3 grown along the (0001) direction. These films show a Morin transition at T_M = 200 K which is hysteretic in nature[20] (details of the growth, see supplemental), below which $\boldsymbol{n}$ is aligned along the *c*-axis, which is out of the plane as shown schematically in Fig. 1a (along $\boldsymbol{z}$ for $T < T_M$) .

When a charge current I_{inj} flows through the Pt injector of a non-local structure (Fig. 1a and details in supplemental), a transverse spin current is created due to the spin Hall Effect (SHE) and a spin-bias $\boldsymbol{\mu_s}$ builds up at the Pt/α-Fe_2O_3 interface[21]. This spin-bias results in the excitation or annihilation of spin-

polarized magnons[7,22]. The magnonic spin current flowing in the antiferromagnet is then absorbed by a Pt detector, whereby it is converted to a charge current via the inverse SHE. This spin-bias signal can then be expressed as a non-local resistance ($R_{el} = V_{el}/I_{inj}$).

We measured R_{el} for selected different antiferromagnetic configurations with the magnetic fields in the sample plane, parallel to the wires (which are parallel to ***x***) and out of the plane, along the easy-axis (along ***z***), Fig. 1. Here, we focus on measurements performed at 175 K, below T_M, in the easy-axis phase where we can stabilize and propagate circularly-polarized magnons.

For a field applied along ***y,*** perpendicular to the non-local structure, as well as at zero-field, we observe

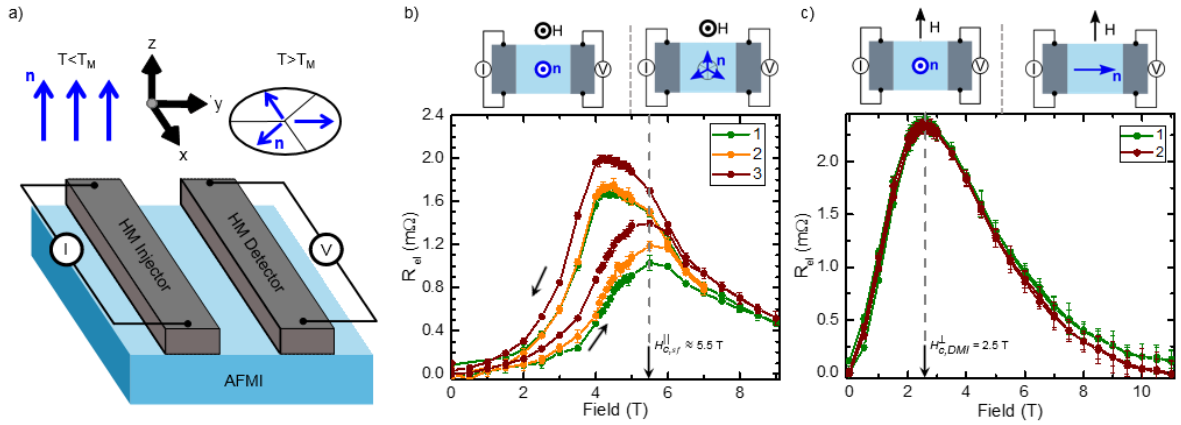

Fig. 1: Non-local measurements of spin-transport in a (0001) oriented films of hematite at 175 K. *a) Schematic of the used non-local geometry of platinum wires on top of an antiferromagnetic insulator thin film. The electrical contacts and axes are indicated as well as the relative orientation of the Néel vector (blue) in respectively the easy-axis ($T<T_M$) and easy-plane ($T>T_M$) phases (here assuming an additional threefold in-plane anisotropy). b) Spin-bias signal for* ***H****||****z****. The spin-bias signal displays a hysteretic-like behavior due to an additional magnetic anisotropy of magnetoelastic origin above* $\mu_0 H_{c,sf}^{||} \approx 5.5$ T *that needs to be overcome when lowering the field and shows a training effect with field cycling (1-3) that is reset when warmed above* T_M*. c) Spin-bias signal for* ***H****||****x****. The spin-bias signal increases up to* $\mu_0 H_{c,DMI}^{\perp} = 2.5$ T*, where the Néel vector* ***n*** *is aligned along* ***y****. This orientation shows no training effect or hysteresis.*

no spin-bias signal arising from the injected spins as in all these cases $\boldsymbol{n} \perp \boldsymbol{\mu}_s$. On the contrary, maximal

signals for R_{el} are observed for magnetic fields perpendicular to the wires in ferromagnetic materials[22]. For a field **H**||***z*** (Fig. 1.b), we observe the spin-flop transition at around $\mu_0 H_{c,sf}^{||} \approx 5$ T, above which ***n*** lies in the sample plane (see Fig. 1.a). The transmitted signal reaches a maximum in close vicinity to $H_{c,sf}^{||}$. As the field is reduced back to zero, we see a hysteresis like behavior emerging, where the R_{el} is larger for some field range than for the increasing field branch. By repeated field cycling, we also see a clear training effect, where the peak amplitude increases and the transition width becomes sharper with successive cycles indicating changes in the magnetic properties and demonstrating that the transfer of spin-information can be tuned by magnetic field effects.

We ascribe this enhancement of the transport to the strong induced softening of one of the magnon modes[7,13,23] in the vicinity of spin-flop transition and the corresponding increase of the magnon population as the magnon gap is reduced. Below $H_{c,sf}^{||}$, $\boldsymbol{n} \perp \boldsymbol{\mu}_s$ and the signal is suppressed whilst in the transition region around $H_{c,sf}^{||}$, ***n*** has a non-zero projection on $\boldsymbol{\mu}_s$ leading to a pronounced contribution to the signal. As the field is further increased ($H > H_{c,sf}^{||}$), the excited magnons adopt a linear polarization, the magnon gap opens and the signal diminishes.

The hysteretic behavior observed, along with the training effect in these (0001) thin films is distinctly different from the behavior found previously for single crystals[7]. We can explain this behaviour by the particular geometry where the field is applied along the easy-axis perpendicular to the surface not previously measured for single crystals. This leads to the formation of non-180^0 domains above the spin-flop transition due to the 3-fold degeneracy of ***n*** in the easy-plane phase when **H**||***z*.** Successive field cycles through the spin-flop transition lead to depinning and annihilation of domains walls, and given the pronounced increase of the signal this is a first indication that the spin-transport depends on the domain configuration. The domain formation above the spin-flop is dominated by the magnetostrictive interaction, which can be sizeable in hematite[24,25], and additionally imperfections of the substrate as the growth seed can have an effect. Such an additional magnetostrictive-induced anisotropy above $H_{c,sf}^{||}$ leads to a pinning potential that must be overcome when the magnetic field is lowered thus leading to the hysteretic signal due to hysteretic changes in the domain structure. From a

hysteresis width of ~ 1.5 T, we calculate a uniaxial anisotropy field of 30 mT and magnetostrictive field of 8 mT. From this, we can estimate the strength of the pinning to be $8 \times 10^2 \frac{J}{m^3}$ in agreement with literature values on bulk samples[25] (see model in supplemental).

Beyond this first geometry of the applied field direction, we next apply the field along the wires, **H**||***x*** (see Fig. 1c). We also observe a spin-bias signal in this geometry. We note that a spin-reorientation for $\boldsymbol{H} \perp \mathbf{EA}$ occurs in easy-axis antiferromagnets with a Dzyaloshinskii-Moriya interaction (DMI)||**EA** [26], and it is a smooth second-order transition, unlike the hysteretic spin-flop transition at $H_{c,sf}^{||}$ [27]. This allows us to draw strong parallels to magnetic field transitions along respectively the hard and easy-axis of a ferromagnet. From zero-field to a critical field $H_{c,DMI}^{\perp}$, the spins smoothly rotate and tend to align perpendicular to both the external field and the DMI vector (||**EA**). This leads to a progressive parallel alignment of $\boldsymbol{n}$ and $\boldsymbol{\mu}_s$, accompanied by the softening of one magnon mode[27,28]. Similarly to the **H**||***z*** case, these two features explain the increasing signal up to $H_{c,DMI}^{\perp}$ where $\boldsymbol{n}||\boldsymbol{\mu}_s$. The signal is furthermore exhibiting a π periodicity of the angle between $\boldsymbol{n}$ and $\boldsymbol{\mu}_s$ (supplemental). Above this critical field of the spin-reorientation, the signal again decreases at large fields due to the emergent linearly-polarized magnons and an opening of the magnon gap[27,28]. In contrast to the case **H**||***z*,** no additional domain structure is formed when **H**||***x*,** as the equilibrium orientation of **n** is nondegenerate, leading to the absence of any hysteresis or training effects.

A magnonic spin current is transmitted when $\boldsymbol{\mu}_s$ and $\boldsymbol{n}$ are parallel, however, in the (0001) oriented films this requires the application of high magnetic fields. Such fields are impractical and inefficient for applications that make use of antiferromagnetic components, in addition to the problem of the ambiguity of the signal in the "flopped" state for **H**||**EA**. Therefore, rather than using magnetic fields to align $\boldsymbol{n}$ and $\boldsymbol{\mu}_s$, a zero-field projection would be more practical for antiferromagnetic transport applications.

Therefore we next grow $(1\bar{1}02)$ (r-plane) oriented thin films of hematite which exhibit a Morin-temperature T_M=200 K, (supplementary) and have both a stable surface termination[29] and a zero-field projection of $\boldsymbol{n}$ onto the surface plane. For wires perpendicular to the **EA** projection (Fig. 2a), a parallel alignment of $\boldsymbol{n}$ and $\boldsymbol{\mu}_s$ is possible below the spin-reorientation. Thus, we can study potential zero-field

transport as a function of external field perpendicular (**H**||***x***, Fig. 2b) and parallel (**H**||***y***, Fig. 2c) to the wires. A significant signal is observed even at zero-field where the magnon polarizations have a nonzero projection on $\boldsymbol{\mu}_s$. With increasing field the signal increases until ***n*** rotates perpendicular to **H**[30] and the field dependence shows no training effect or hysteresis. The suppression of the signal with increasing field above the spin-flop transition has the same origin as for the previously discussed (0001) growth orientation.

This crystallographic orientation thus highlights that an efficient magnonic transport is possible through a careful choice of geometry, even without an applied field.

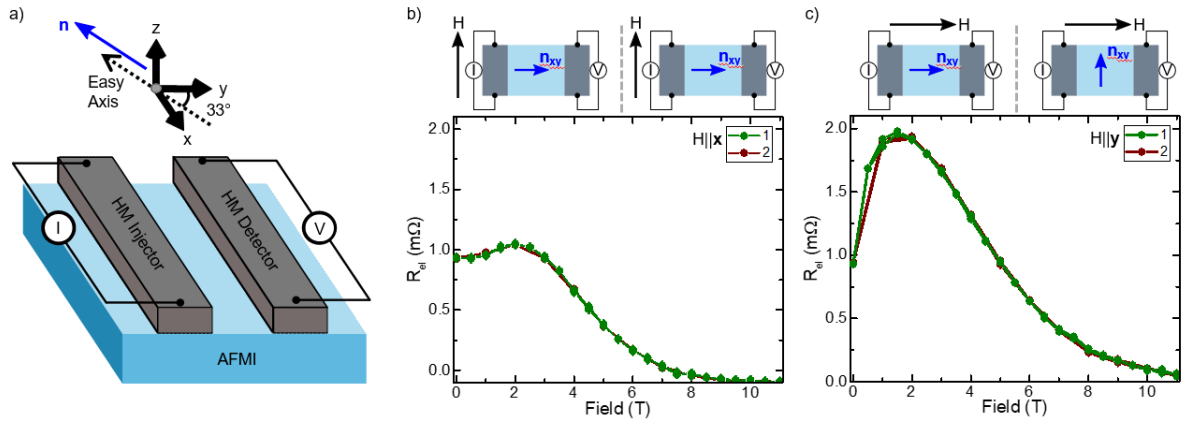

Fig. 2: Non-local transport in (1$\bar{1}$02) hematite at 175 K for wires perpendicular to the easy-axis. *a) Sketch of non-local geometry with respect to the magnetic axis. The **EA** is tilted 33° in the **yz** plane, indicated by the dashed line. The Néel vector lies parallel to the **EA** at zero-field. b,c) Spin-bias for (1$\bar{1}$02) hematite with wires perpendicular to the projection of the **EA**. The field is directed along b) **H**||**x** and c) **H**||**y** for two cycles (1,2). There exists a significant spin-bias signal at zero-field that is suppressed at high fields as the Néel order rotates. There is no observed training effect or hysteresis for this geometry. The error bars are the standard deviation of the data points.*

The key question is the propagation length, as for device applications, information needs to be transported across sufficient distances. While previously transport in thin film antiferromagnets has

only been possible over few nm distances, as shown in Figure 3, we can transport spins here over µm (the value of R_{el} was recorded at both $H_{c,sf}^{||}$ and $H_{c,DMI}^{\perp}$ in the (0001) films whilst for the $(1\bar{1}02)$ films, the value at μ_0H = 1.5 T for **H**||**x** and **H**||**y** is taken to remove any possible interfacial canting[31]). The lack of a threshold and the used elevated temperature of 175 K indicate that diffusive transport dominates[7], allowing us to use a one-dimensional spin-diffusion-relaxation equation to estimate the spin-diffusion lengths in our films[22]. We find for (0001) and $(1\bar{1}02)$ samples for the three selected geometries: $\lambda_{c,DMI}^{\perp} = 400\,nm$, $\lambda_{r,1.5\,T}^{x} = 600\,nm$, and $\lambda_{r,1.5\,T}^{y} = 800\,nm$, which is two orders of magnitude greater than previous reports for epitaxial[8] or polycrystalline[9] thin film antiferromagnets. However, one must also note that the distance dependence of R_{el} at $H_{c,sf}^{||}$ cannot be fit with a simple 1D spin-diffusion due to the hysteretic behavior and the observed training effect (inset of Fig. 3a). Together with the observation that the signal during the hysteretic behavior depends on the field cycling which affects the spin structure, this raises the major open question of the origin of the transport of magnons across distances far larger than previously observed in thin film antiferromagnets. Furthermore, there is the question of why the spin-transport length-scales vary so strongly even within a single material and is not described for all geometries by a simple diffusion model[22].

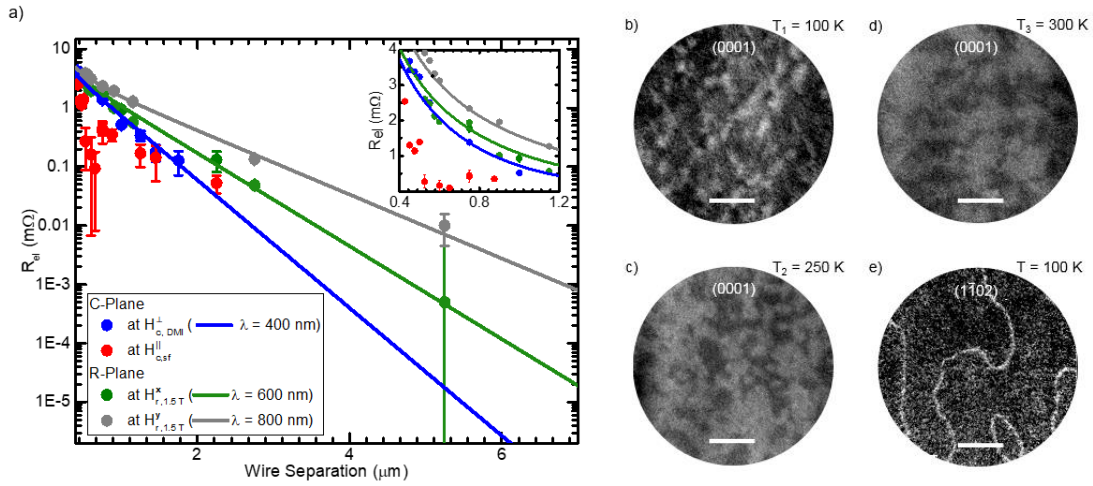

Fig. 3: Distance dependence of R_{el} and X-ray magnetic linear dichroism-photoemission electron microscopy (XMLD-PEEM) images of hematite thin films *a) Distance dependence of non-local resistance for (0001) hematite at both $H_{c,sf}^{||}$ (red) and $H_{c,DMI}^{\perp}$ (blue) as well as $1\bar{1}02$ hematite for a field directed along **x** (green) and **y** (grey) along with fits to the one-dimensional spin-diffusion equation. Inset shows the spin-bias signal for low distances. The error bars represent the standard deviation of the data. For $H_{c,sf}^{||}$ the error bars represent the standard deviation of multiple field cycles. The curve at $H_{c,sf}^{||}$ (red) is the average across many successive field cycles for each device at the peak field for the lowering field sweep. b)-d) XMLD-PEEM image of 100 nm thick (0001) hematite at T_1 = 100 K, T_2 = 250 K and T_3 = 300 K, and $\mu_0 H$ = 0 T. e) XMLD-PEEM imaging of 500 nm (1102) hematite at T = 100 K, below the Morin transition, and $\mu_0 H$ = 0* T. *Large, micrometer sized domains are separated by clear 180° domain walls. The scale bars represent 2 μm.*

To analyze the mechanisms that govern the propagation lengths, we consider two factors. The decay of magnons due to magnetic damping leads to an attenuation that is, in the simplest model, independent of the spin structure. Additionally, scattering of magnons is predicted to occur at magnetic domain walls [32,33] leading to a spin-structure dependent propagation length. To investigate these factors, we performed X-ray magnetic linear dichroism photoelectron emission (XMLD-PEEM) imaging at the Fe L2 edge (details, see supplemental). Whilst the domain structure of the $(1\bar{1}02)$ films at zero-field can be imaged directly, the domain structure in the (0001) films at either $H_{c,sf}^{||}$ and $H_{c,DMI}^{\perp}$ cannot be directly observed due to the need for high magnetic fields that cannot be applied during PEEM imaging. However, the type of domain structure at the spin-flop field can be obtained by instead imaging the spin-structure above T_M, where the magnetic state is also in the easy-plane and energetically a similar situation is attained[26]. For the (0001) films, we observe in Fig 3b-3d (100 K – 300 K) a multi-domain pattern. Above T_M (Fig 3d) we find domain sizes of a few hundred nanometers. When we reduce the temperature, the domain spin structure changes strongly across the Morin transition. Surprisingly, we still measure a contrast from magnetic domains below T_M (see Fig 3.b) where the spin-structure should be in the easy-axis phase, and 180° domains should lead to the same dichroic signal and the absence of contrast. We associate this contrast to a distribution of the growth crystallites leading to an off-axis

component of $\boldsymbol{n}$ (supplemental). However, we can infer the presence of 180° domain walls below T_M from the clear observation in the $(1\bar{1}02)$ films (see Fig. 3.e) later[34]. Whilst the domain structure above T_M gives an indication of the magnetic state at $H_{c,sf}^{||}$, no direct, quantitative way exists to access the magnetic state at $H_{c,DMI}^{\perp}$. Nevertheless, the domains are expected to be similarly sized and lack degeneracy at $H_{c,DMI}^{\perp}$, as evidenced by the non-hysteretic transport signal (Fig.1.c), separated by 180° domain walls.

In the $(1\bar{1}02)$ films, we observe below T_M and at zero-field that 180° domain walls separate large single domain areas and the contrast is larger than for the (0001) orientation due to the inclination of the easy-axis. To our knowledge, the clear observation of 180° antiferromagnetic domain walls in antiferromagnetic films has not been reported, although 90° domain walls have been observed[35]. The size of the domains is of the order of many micrometers, an order of magnitude larger than in the (0001) orientation. The $(1\bar{1}02)$ films thus show not only longer propagation lengths than (0001) films but also larger antiferromagnetic domains, highlighting the relation between the domain structure and the spin-transport.

To understand this behavior, we discuss the propagating magnonic spin current properties and its interaction with domains and domain walls. The magnons are excited with a broad spectrum of energy and wavevector ($\boldsymbol{k}$) with an upper limit determined by thermal energy. Within a single domain, the magnon propagation length is mainly determined by spatial diffusion and the magnetic damping. However, the presence of domain walls can introduce extra dissipation channels through spin-dependent scattering [32,33,36]. This can reduce the propagation length of the magnons and experimentally lead to an attenuation of the signal. At 60° domain walls, such as above $H_{c,sf}^{||}$, magnons scatter due to the Néel order reorientation between the neighboring domains. For circularly-polarized magnons, as in the easy-axis phase of hematite, we develop a simple toy model of the scattering process at a 180° domain wall pinned by a homogeneous distribution of defects acting to fix the orientation of $\boldsymbol{n}$ in the center of the domain wall (model details, see supplemental). From this model, we find that the scattering is significant up to a critical value of the wavenumber, $\boldsymbol{k_{crit}}$, which is proportional to the pinning field

obtained from the experimental data. For large pinning, all types of AFM magnons can scatter from the domain walls and the propagation length is dominated by the domain size.

This model now allows us to explain the observed transport: with magnetic domains larger than the diffusion length, the magnon transport obeys a 1D diffusive model in the $(1\bar{1}02)$ films. In in the (0001) films, with the presence of many domain walls that act as scattering sites, the signal attenuates over shorter distances where the size of the domains serve to define the characteristic decay length. The small domains previously observed in thin film antiferromagnets[3,34,35] thus prove detrimental to the transport of spin information and we highlight here that the functionalization of antiferromagnetic spintronic devices strongly benefits from the absence of antiferromagnetic domain walls.

The transport of spin-information in antiferromagnetic thin films with large magnetic domains can then reach micrometers, as in the best ferromagnetic thin film systems[22], which opens the way for instance towards the development of antiferromagnetic spin-logic devices[37]. An applied magnetic field can be used to both train the domain structure and control the orientation of the Néel vector in order to facilitate the detection and tune the transport efficiency of magnons. For selected growth orientations, a zero-field projection of the Néel vector can be achieved leading to field free spin-transport. These different approaches to control magnon transports offer multiple routes to the application of antiferromagnets in magnonic devices[37].

Acknowledgements
The authors acknowledge thoughtful input and discussion with David Ellis. A.R., G.J., and M.K. acknowledge support from the Graduate School of Excellence Materials Science in Mainz (DFG/GSC 266). A. R., R. L. and M.K. acknowledge support from the DFG project number 423441604. R.L. acknowledges the European Union's Horizon 2020 research and innovation programme under the Marie Skłodowska-Curie grant agreement FAST number 752195. S.B. and G.J from DFG project number 358671374. O.G. and J.S. acknowledges the support from the Humboldt Foundation, the ERC Synergy Grant SC2 (No. 610115), the EU FET Open RIA Grant no. 766566. O.G. additionally acknowledges the DFG (project SHARP 397322108). D.G., A.K. and Av.R. acknowledges support from the European Research Council under the European Union's Seventh Framework programme (FP/200702013) / ERC (Grant Agreement No. 617516). L. B. acknowledges the European Union's Horizon 2020 research and innovation programme under the Marie Skłodowska-Curie grant agreement ARTES number 793159. All authors from Mainz also acknowledge support from both MaHoJeRo (DAAD Spintronics network, project number 57334897) and SPIN+X (DFG SFB TRR 173, projects A01 and B02). A.Q. and A.B. acknowledge support from the European Research Council via Advanced Grant number 669442 'Insulatronics'. A.Q., C. U., R.A.D., M.K. and A.B. were supported by the Research Council of Norway through its Centres of Excellence funding scheme, project number 262633 'QuSpin'.

Author contributions

R.L. and M.K. proposed and supervised the project. A.R. performed with R.L the transport experiments. R.L, L. B and F.K performed the XMLD-PEEM measurements and analyzed the data with A.R. A.R. patterned with R.L. the samples. D. G, A. K and Av. R grew and optimized the films. A. R., R.L and S.B performed the XRD and SQUID measurements with input from G. J. O.G, C.U. and A.Q. developed theoretical understanding with assistance and input from J.S., R.D and A.B. A.R and R.L. analyzed the data with inputs from M.K. and O.G. A. R and R.L wrote the paper with M.K and O. G.. All authors commented on the manuscript.

1. Baltz, V. *et al.* Antiferromagnetic spintronics. *Rev. Mod. Phys.* **90**, 015005 (2018).
2. Jungwirth, T. *et al.* The multiple directions of antiferromagnetic spintronics. *Nat. Phys.* **14**, 200–203 (2018).
3. Baldrati, L. *et al.* Full angular dependence of the spin Hall and ordinary magnetoresistance in epitaxial antiferromagnetic NiO(001)/Pt thin films. *Phys. Rev. B* **98**, 024422 (2018).
4. Hoogeboom, G. R., Aqeel, A., Kuschel, T., Palstra, T. T. M. & van Wees, B. J. Negative spin Hall magnetoresistance of Pt on the bulk easy-plane antiferromagnet NiO. *Appl. Phys. Lett.* **111**, 052409 (2017).
5. Bodnar, S. Y. *et al.* Writing and reading antiferromagnetic Mn_2Au by Néel spin-orbit torques and large anisotropic magnetoresistance. *Nat. Commun.* **9**, 348 (2018).
6. Chen, X. Z. *et al.* Antidamping-Torque-Induced Switching in Biaxial Antiferromagnetic Insulators. *Phys. Rev. Lett.* **120**, 207204 (2018).
7. Lebrun, R. *et al.* Tunable long-distance spin transport in a crystalline antiferromagnetic iron oxide. *Nature* **561**, 222–225 (2018).
8. Baldrati, L. *et al.* Spin transport in multilayer systems with fully epitaxial NiO thin films. *Phys. Rev. B* **98**, 14409 (2018).
9. Wang, H., Du, C., Hammel, P. C. & Yang, F. Spin transport in antiferromagnetic insulators mediated by magnetic correlations. *Phys. Rev. B* **91**, 220410 (2015).
10. Cramer, J. *et al.* Spin transport across antiferromagnets induced by the spin Seebeck effect. *J. Phys. D. Appl. Phys.* **51**, 144004 (2018).
11. Keffer, F. & Kittel, C. Theory of Antiferromagnetic Resonance. *Phys. Rev.* **85**, 329–337 (1952).
12. Bender, S. A., Skarsvåg, H., Brataas, A. & Duine, R. A. Enhanced Spin Conductance of a Thin-Film Insulating Antiferromagnet. *Phys. Rev. Lett.* **119**, 056804 (2017).
13. Gurevich, A. G. & Melkov, G. A. *Magnetization Oscillations and Waves*. (CRC Press, 1996).
14. Cantalini, C., Faccio, M., Ferri, G. & Pelino, M. Microstructure and electrical properties of Si-doped α-Fe_2O_3 humidity sensor. *Sensors Actuators B Chem.* **16**, 293–298 (1993).
15. Dotan, H. *et al.* Resonant light trapping in ultrathin films for water splitting. *Nat. Mater.* **12**, 158–164 (2013).
16. Morin, F. J. Magnetic Susceptibility of α-Fe_2O_3 and α-Fe_2O_3 with Added Titanium. *Phys. Rev.* **78**, 819–820 (1950).
17. Morrish, A. H., Johnston, G. B. & Curry, N. A. Magnetic transition in pure and Ga doped α-Fe_2O_3. *Phys. Lett.* **7**, 177–178 (1963).

18. Grave, D. A. *et al.* Effect of Orientation on Bulk and Surface Properties of Sn-doped Hematite (α-Fe_2O_3) Heteroepitaxial Thin Film Photoanodes. *J. Phys. Chem. C* **120**, 28961–28970 (2016).

19. Grave, D. A. *et al.* Heteroepitaxial hematite photoanodes as a model system for solar water splitting. *J. Mater. Chem. A* **4**, 3052–3060 (2016).

20. Shimomura, N. *et al.* Morin transition temperature in (0001)-oriented α-Fe_2O_3 thin film and effect of Ir doping. *J. Appl. Phys.* **117**, 17C736 (2015).

21. Sinova, J., Valenzuela, S. O., Wunderlich, J., Back, C. H. & Jungwirth, T. Spin Hall effects. *Rev. Mod. Phys.* **87**, 1213–1260 (2015).

22. Cornelissen, L. J., Liu, J., Duine, R. A., Youssef, J. Ben & Van Wees, B. J. Long-distance transport of magnon spin information in a magnetic insulator at room temperature. *Nat. Phys.* **11**, 1022–1026 (2015).

23. Besser, P. J. & Morrish, A. H. Spin flopping in synthetic hematite crystals. *Phys. Lett.* **13**, 289–290 (1964).

24. Morrish, A. H. *Canted Antiferromagnetism : Hematite*. (World Scientific Pub Co Inc, 1995). doi:10.1142/2518

25. Levitin, R. Z., Pakhomov, A. S. & Shchurov, V. A. Magnetoelastic properties of hematite. *Sov. Phys. JETP* **29**, 669-673 (1969) [Zh. Eskp. Teor. Fiz. 56, 1242-1251 (1969)].

26. Flanders, P. J. & Shtrikman, S. Magnetic field induced antiferromagnetic to weakferromagnetic transitions in hematite. *Solid State Commun.* **3**, 285–288 (1965).

27. Morrison, B. R., Morrish, A. H. & Troup, G. J. High-Field Antiferromagnetic Resonance in α-Fe_2O_3. *Phys. Status Solidi* **56**, 183–195 (1973).

28. Ozhogin, V. I. & Shapiro, V. G. New Type of Antiferromagnet Resonance in α-Fe_2O_3. *JETP Lett* **6**, 7 (1967) [ZhETF Pis'ma 6, 1, 467-471 (1967)].

29. Kraushofer, F. *et al.* Atomic-Scale Structure of the Hematite α-Fe_2O_3 $(1\bar{1}02)$ "R-Cut" Surface. *J. Phys. Chem. C* **122**, 1657–1669 (2018).

30. Lebrun, R. *et al.* Anisotropies and magnetic phase transitions in insulating antiferromagnets determined by a Spin-Hall magnetoresistance probe. *Commun. Phys.* **2**, 50 (2019).

31. Vélez, S., Bedoya-Pinto, A., Yan, W., Hueso, L. E. & Casanova, F. Competing effects at Pt/YIG interfaces: Spin Hall magnetoresistance, magnon excitations, and magnetic frustration. *Phys. Rev. B* **94**, 174405 (2016).

32. Lan, J., Yu, W. & Xiao, J. Antiferromagnetic domain wall as spin wave polarizer and retarder. *Nat. Commun.* **8**, 178 (2017).

33. Yu, W., Lan, J. & Xiao, J. Polarization-selective spin wave driven domain-wall motion in antiferromagnets. *Phys. Rev. B* **98**, 144422 (2018).

34. Appel, P. *et al.* Nanomagnetism of Magnetoelectric Granular Thin-Film Antiferromagnets. *Nano Lett.* **19**, 1682–1687 (2019).

35. Wadley, P. *et al.* Current polarity-dependent manipulation of antiferromagnetic domains. *Nat. Nanotechnol.* **13**, 362–365 (2018).

36. Tveten, E. G., Qaiumzadeh, A. & Brataas, A. Antiferromagnetic Domain Wall Motion Induced by Spin Waves. *Phys. Rev. Lett.* **112**, 147204 (2014).

37. Chumak, A. V., Vasyuchka, V. I., Serga, A. A. & Hillebrands, B. Magnon spintronics. *Nat. Phys.* **11**, 453–461 (2015).